Journal of Biomechanics 130 (2022) 110873

Contents lists available at ScienceDirect

Journal of Biomechanics

journal homepage: www.elsevier.com/locate/jbiomech

Personalised nitinol stent for focal plaques: Design and evaluation

Ran He [a,*], Liguo Zhao [a], Vadim V. Silberschmidt [a], Jiling Feng [b], Ferdinand Serracino-Inglott [c]

[a] Wolfson School of Mechanical, Electrical and Manufacturing Engineering, Loughborough University, Epinal Way, Loughborough LE11 3TU, UK
[b] Department of Engineering, Manchester Metropolitan University, Manchester M15 6BH, UK
[c] Manchester Academic Health Science Centre, Manchester University NHS Foundation Trust, Manchester, UK

ARTICLE INFO

Keywords:
Femoropopliteal artery
Finite element
Focal plaque
Nitinol stent
Personalised design

ABSTRACT

The purpose of this study is to develop personalised nitinol stents for arteries with one and two opposite focal plaques. Novel designs are evaluated through comparison with a commercial stent design, in terms of lumen gain and shape as well as stress levels in the media layer after stenting. Methods: Personalised stents are developed for arteries with one and two opposite focal plaques, based on medical imaging of patients and computer simulations. In silico analysis is then carried out for assessment of stent performance in the diseased arteries. Results: Personalised designs significantly increase the lumen gain, reduce the stresses in the media layer, and improve the lumen shape compared to the commercial nitinol stent. Conclusion: The personalised designs show outstanding performance compared to the commercial stent. Significance: This pilot study proves that personalised nitinol stents are able to deliver desirable treatment outcomes.

1. Introduction

Self-expandable stents, made of nickel-titanium alloy (nitinol), are used to treat atherosclerosis in femoropopliteal arteries. They can expand by themselves without using a balloon (as with other stent materials) and recover from deformations caused by limb flexion thanks to the superelastic behaviour of nitinol. Compared to balloon angioplasty alone, the rate of arterial recoil and in-stent restenosis can be reduced by the self-expandable nitinol stents (Fusaro et al., 2013; Laird et al., 2010; Schillinger et al., 2006). However, the designs of commercial stents currently available on the market are uniform, with repeating patterns. Meanwhile, actual plaques can be highly irregular and vary in different patients (von Birgelen et al., 2001). Thus, desired treatment outcomes of such stenosis cannot be produced with the uniform stent designs. The next-generation stents should be designed with consideration of the lesion-specific nature of the stenosis (Ako et al., 2007). Moreover, multiple plaque lesions can exist in the same vessel and be very close to each other (He et al., 2019; Torres Lebruno et al., 2020). This is very common in the superficial femoral artery. A single uniform-design stent is usually used to treat such lesions in clinical practice. The disadvantages of the uniform stent design include over-expansion of the healthy regions between the plaques as well as over-expansion of the healthy side of the artery (i.e., with no or very thin plaque), which increase the risk of tissue damage, associated with in-stent restenosis.

Efforts were made to optimise the designs of balloon-expandable stents. A three-parameter technique was proposed by Pant et al. (2011, 2012) to optimise the design of a CYPHER stent, in order to improve its performance in terms of stent recoil, tissue stress, haemodynamic disturbance, delivery and distribution of drug, and mechanical flexibility. They demonstrated that an improvement in one objective often came along with a compromise of other objectives. Recently, Ribeiro et al. (2021) optimised a coronary PROMUS Element stent with reduced vessel injury, radial recoil, and prolapse as well as improved bending, longitudinal, and radial strength, by the use of a zero, or nearly zero, height of connecting bridges. The strut width, thickness, and length of a bioresorbable polymeric coronary stent was optimised using a similar approach in Blair et al. (2019) to improve its performance in terms of post-dilation, foreshortening, stent-to-artery ratio, and radial collapse pressure. The authors also found that an improved metric often came along with a compromise of other metrics as in Pant et al. (2011, 2012). A topology optimisation approach was used by Khan et al. (2017) to optimise the geometry of a polymeric stent for plaques with different stenosis rates and compositions. Compared with a generic stent, a lower recoil was achieved by their designs. Although designing personalised stent based on the lesion profile is potentially achievable with this approach, no promising results were produced by their designs.

The designs of self-expandable nitinol stents were also explored by

* Corresponding author.
E-mail address: r.he2@lboro.ac.uk (R. He).

https://doi.org/10.1016/j.jbiomech.2021.110873
Accepted 16 November 2021
Available online 23 November 2021

using the parametric optimisation. Azaouzi et al. (2013) improved the fatigue performance of a nitinol stent by using such methodology. They managed to minimise the strut volume whilst maintaining the radial force and the strain amplitude of the stent above a threshold and a strain amplitude below a critical value, respectively. A multi-objective optimisation methodology was used by Amirjani et al. (2014) to improve the designs of stents made of 316L stainless steel and nitinol with a larger apex width, resulting in a reduced stress. A parametric optimisation framework was also proposed by Alaimo et al. (2017) for nitinol stent design, to increase the fatigue performance of the stents. They confirmed that the use of a tapered strut profile could reduce and smoothen the strain field along the strut, enhancing the fatigue life of the stent. However, the optimised designs in these studies were all uniform, and there is a severe lack of studies on developing personalised stents.

This study developed personalised nitinol stents for arteries with one and two opposite focal plaques derived from clinical imaging. Computer simulations were carried out for stent expansion and deployment procedures. The performance of the developed personalised nitinol stents was compared with that of a commercial nitinol stent, in terms of lumen gain and shape as well as stresses in the media layer after stenting.

2. Constitutive models

2.1. Hyperelastic model for plaque

The first-order Ogden hyperelastic model (Ogden, 1972) was used to describe the constitutive behaviour of the plaque (assumed to be isotropic), for which the pseudo-energy potential is given as

$$\psi = \frac{1}{D}(J-1)^2 + \frac{2\mu}{\alpha^2}\left(\bar{\lambda}_1^{\alpha} + \bar{\lambda}_2^{\alpha} + \bar{\lambda}_3^{\alpha} - 3\right), \tag{1}$$

where μ , α and D are the material parameters, J is the volumetric ratio, λ_1 , λ_2 and λ_3 are the principal stretches (ratios), and the bar denotes isochoric values.

The model parameters were determined by fitting the experimental stress-stretch data obtained in Maher et al. (2011) for echolucent plaque, and the corresponding values are given in Table 1, where ρ is the density of the plaque with the value from Rahdert et al. (1999).

2.2. HGO-C model for arterial layers

The HGO-C model (Dassault Systèmes, 2017; Gasser et al., 2006; Holzapfel et al., 2000) was used to describe the anisotropic hyperelastic constitutive behaviour of arterial layers, with a pseudo-energy potential given by

$$\psi = \frac{1}{D}\left(\frac{J^2-1}{2} - \ln J\right) + C_{10}(\bar{I}_1 - 3) + \frac{k_1}{2k_2}\sum_{\alpha=1}^{N}\left[\exp\left(k_2\langle\bar{E}_{\alpha}\rangle^2\right) - 1\right], \tag{2}$$

with

$$\bar{E}_{\alpha} \overset{\text{def}}{=} \kappa(\bar{I}_1 - 3) + (1-3\kappa)\left[\bar{I}_{4(\alpha\alpha)} - 1\right], \tag{3}$$

where C_{10} and k_1 are the stress-like parameters, k_2 is the dimensionless parameter, $\langle\rangle$ stands for the Macaulay brackets, κ $(0 \le \kappa \le 1/3)$ is the temperature-dependent material parameter describing the level of dispersion in the fibre directions, N is the number of families of fibres $(N \le 3)$, I_1 is the first principal invariant of the right Cauchy–Green deformation tensor $\mathbf{C}$ (i.e., $I_1 = \mathrm{tr}\mathbf{C} = \lambda_1^2 + \lambda_2^2 + \lambda_3^2$ and its isochoric part is $\bar{I}_1 = J^{-2/3}I_1$), $I_{4(\alpha\alpha)}$ are the invariants of $\mathbf{C}$ and $\mathbf{a}_{\alpha}$ (i.e., $I_{4(\alpha\alpha)} = \mathbf{a}_{\alpha}\bullet\mathbf{C}\mathbf{a}_{\alpha}$, with $\mathbf{a}_{\alpha}$ being the unit vectors used to define the mean directions of fibres in the reference configuration).

The model parameters were provided in Fereidoonnezhad et al. (2016) and determined by fitting the experimental stress-stretch data measured in Weisbecker et al. (2012). In this study, it was assumed that there were two families of fibres, embedded symmetrically in the tangential surface of each arterial layer (no components in the radial direction), with φ being the angle between the mean direction of fibres and the circumferential direction in the artery. This was based on the work of Schriefl et al. (2012; 2013), who physically observed that the arterial layers had two very distinct counter rotating fibre families, almost symmetrically arranged with respect to the longitudinal axis. In addition, the observed fibre orientations were always in the tangential plane of the walls, with no radial components and very small dispersion through the wall thickness. The parameter values are given in Table 2 for the media and adventitia layers. The extremely thin intima layer was not considered in the simulations due to its negligible contribution to artery deformation (He et al., 2020a).

2.3. Superelastic model for stent

The self-expandable stent considered in this study was made of superelastic nitinol. The equations for its superelastic mechanical model are provided in Auricchio et al. (1997) and Auricchio and Taylor (1997), with model parameters given in Table 3 (Azaouzi et al., 2013). Here, ρ is the density, E_A, υ_A and E_M, υ_M are the Young's moduli and the Poisson's ratios of the austenite and martensite, respectively; ε^L is the uniaxial transformation strain; $\sigma_{tL}^S, \sigma_{tL}^E, \sigma_{tU}^S, \sigma_{tU}^E$ are the stresses, at which the phase transformation starts and ends during loading (subscript L) and unloading (U) in tension, respectively; σ_{cL}^S is the stress, at which the phase transformation begins in compression.

3. Methods

A schematic of the development process for the personalised stent designs in this study is depicted in Fig. 1. It started with proposing designs ideas and checking whether they could improve the stent performance in terms of lumen gain and shape as well as stress in the media layer after stenting. If not, other design ideas would be proposed. When stent performance was improved, personalised stent designs were attained for lesion-specific arteries and their performances were evaluated with the deployment analysis. Here, the design ideas included the circumferentially varying strut width and thickness and the oval shape; they were iterated based on the finite element simulations described below.

Two models were built for arteries with one and two opposite focal plaques. The focal plaque model was constructed with Mimics software from DICOM images of a patient's femoropopliteal plaque using the CT imaging technique (Wang et al., 2021). For the single focal plaque, a model of a straight artery with a 0.5-mm thick and 20-mm long uniform thin-layer plaque was built first in Abaqus and then exported to 3-Matic software. The single focal plaque model, with a maximum thickness of about 2 mm and a length of 20 mm, was then exported from Mimics to 3-Matic and placed on top of the thin-layer plaque to generate the whole model (Fig. 2a). For the double opposite focal plaques, a model of

Table 1
Parameter values of Ogden model for plaque.

ρ (t/mm^3)	μ (MPa)	α	D (MPa^{-1})	r	m (mJ/mm^3)
1.22E-9	0.00396803	13.8367	0.239019	1.3	0.008

Table 2
Parameter values of HGO-C model for arterial layers (Fereidoonnezhad et al., 2016).

Layer	ρ (t/mm^3)	C_{10} (MPa)	D (MPa^{-1})	k_1 (MPa)	k_2	κ	φ (°)
Media	1.07E-9	0.020	0.001	0.112	20.610	0.24	41.0
Adventitia	1.07E-9	0.008	0.001	0.362	7.089	0.17	50.1

Table 3
Parameter values of superelastic model for nitinol (Azaouzi et al., 2013).

ρ (t/mm^3)	E_A (MPa)	υ_A	E_M (MPa)	υ_M	ε^L	σ^S_{tL} (MPa)	σ^E_{tL} (MPa)	σ^S_{tU} (MPa)	σ^E_{tU} (MPa)	σ^S_{cL} (MPa)
6.45E-9	68,000	0.3	36,000	0.3	0.06	520	635	250	150	780

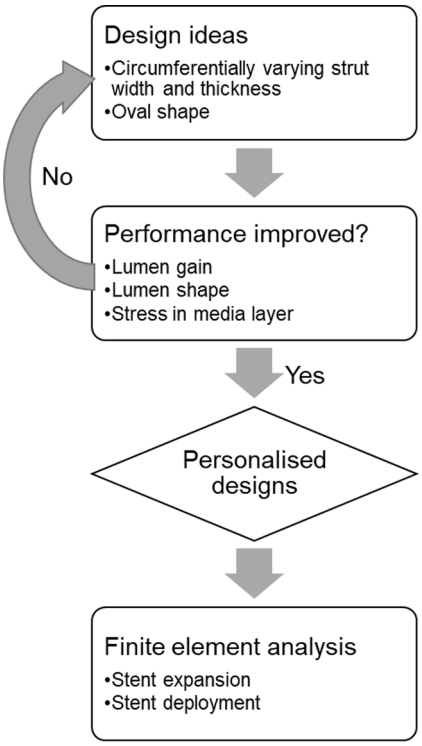

Fig. 1. Flowchart detailing development process of personalised stent designs in this study.

straight artery with two 0.5-mm thick and 7.5-mm long uniform thin-layer plaques and a 5-mm long gap between them was first developed by Abaqus, and then exported to 3-Matic. The two focal plaques were then placed on top of two thin-layer plaques, respectively, but opposite to each other, to generate the whole model (Fig. 2b). Here, the two focal plaques had the same profile, with a maximum thickness of about 2 mm and a length of 7.5 mm. The maximum stenosis rate of both arteries was about 75%. Both arteries had a length of 50 mm and an inner radius of 2 mm, formed by an adventitia and a media layers, with thicknesses of 0.37 mm and 0.83 mm, respectively (Wong et al., 1993). The stents with personalised designs were compared with the commercial nitinol stent (Fig. 2c), having a length of 25 mm, for performance evaluation. Tetrahedral elements (C3D4) were used to mesh the lesion-specific arteries and plaques with 3-Matic software, while C3D8R elements were used to mesh the stents in Abaqus. The stents were meshed with 4 × 4 layers of elements, i.e., 4 layers of elements across the thickness and width of individual strut, respectively. This was based on a mesh sensitivity study in our previous work (Schiavone and Zhao, 2016; Qiu et al., 2018; He et al., 2020a).

To simulate the preparation process, the stent was gradually expanded by applying an outward radial displacement to a linear-elastic tube inside it in the first simulation. Interaction between the stent and the tube was modelled as contact pairs. The second simulation consisted of three steps. In the first step, the artery was pre-dilated by applying a radial displacement to another linear-elastic tube, to place the stent inside the artery. Meanwhile, a third linear-elastic tube was employed to crimp the stent. Interaction between the tube and the stent was added. In the second step, the displacement applied to the pre-dilation tubes were

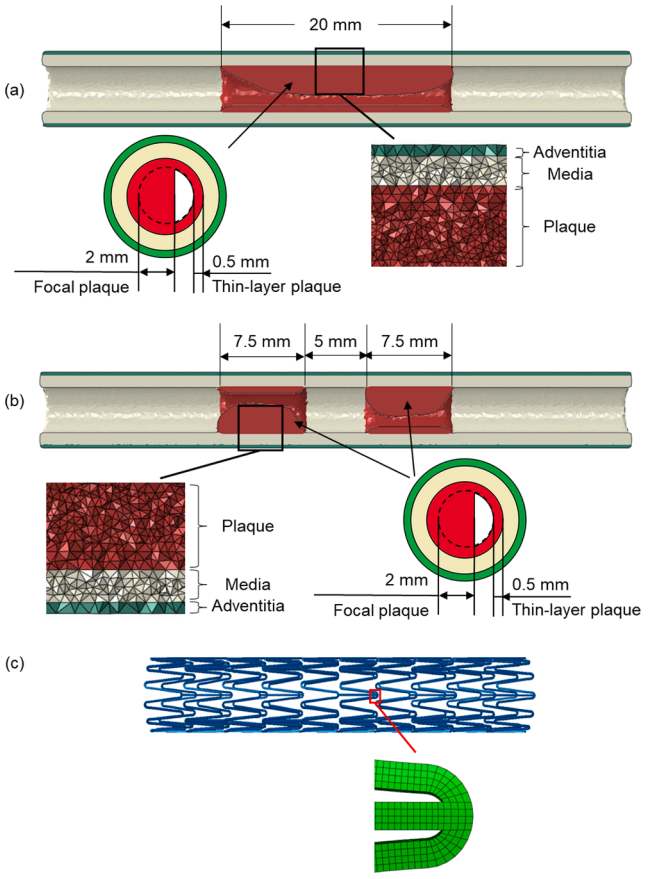

Fig. 2. Finite element models of lesion-specific arteries with (a) one and (b) two opposite focal plaques (adventitia: green; media: beige; plaque: red) with schematics of cross-sectional view of diseased artery and (c) commercial stent.

gradually removed and interaction between the artery and the stent was added. In the final step, the stent was released in the artery, and the interaction between the artery and the pre-dilation tube was removed. Interactions between the arteries, the stents, and the tubes were modelled as general hard contacts with a frictional coefficient of 0.2 (Dordoni et al., 2014). Both ends of arteries were fixed in the longitudinal and circumferential directions throughout the simulations to reduce their effect on the deformations of the diseased arteries and stents. The process of the stent implantation mimicked by the simulations is illustrated in Fig. 3. The simulations were conducted using the Abaqus (2017) explicit solver. The kinetic energy was monitored throughout the simulations to ensure that it did not exceed 5% of the total energy. A mass scaling factor of 1000 and a default damping coefficient of 1.2 for quadratic bulk viscosity was applied in the simulations to increase the computing speed and mitigate high-frequency oscillations, respectively. The increment time for each step in the simulations was in the order of magnitude of 10^{-8} s.

4. Results

4.1. Personalised designs

Design ideas with the circumferentially varying strut width and

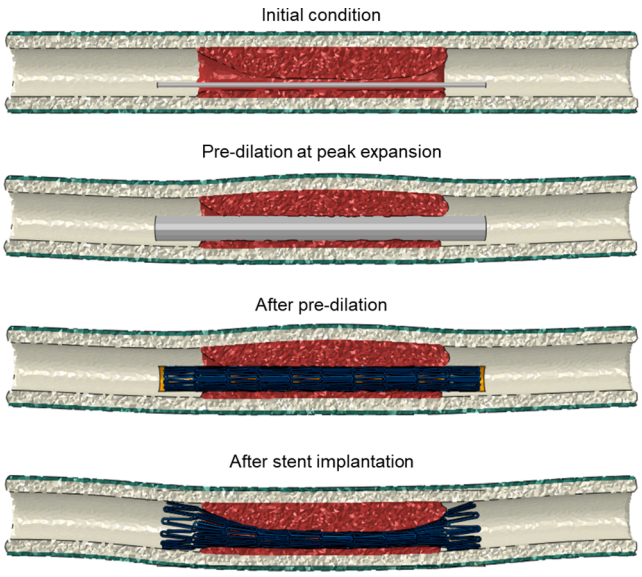

Fig. 3. Process of stent implantation in simulations (adventitia: green; media: beige; plaque: red; tube for pre-dilation: grey; tube for stent crimping and releasing: orange; stent: blue).

thickness and the oval shape were proposed (see Section 1 in Supplementary Material) and used in the personalised stent designs for one and two opposite focal plaques (Fig. 4a and 4b, respectively), to improve the lumen gain and shape and also to reduce the stress in the media layer after stenting. For the single plaque, since its profile was similar in the longitudinal direction, the design was the same for each crown corresponding to the diseased region of the artery. The crown length remained 2.5 mm, the same as that of the commercial nitinol stent. In each crown, four and remaining eight strut units (framed in red and green in Fig. 4a) had widths and thicknesses of 0.074 mm and 0.180 mm, corresponding to the thin-layer and focal plaques, respectively. The change of the strut width/thickness was a gradual process as shown in the zoomed-in inset picture in Fig. 4a (i.e., changed from 0.074 mm to 0.18 mm over the U-bend region). An additional commercial stent crown was added to each end of the designed stent. The semi-major and semi-minor axes (3.48 mm and 1.80 mm, respectively) of the oval shape were determined by its area and the distance between a focus and its closer vertex. The former equalled to the circular area of the commercial stent in the expanded configuration, and the latter equalled to the shortest distance (0.5 mm) between the lumen centre and the inner surface of the thin-layer plaque. Similarly, the personalised stent for the two opposite focal plaques was designed with two sets of three crowns with circumferentially varying width and thickness placed opposite to each other. Besides the commercial stent crown at each end, another two commercial stent crowns were placed in the middle corresponding to the gap between the focal plaques. This design was also expanded to the same oval shape as that for the single plaque.

4.2. Lumen gain

For the cases of one and two opposite focal plaques, the ratio of the lumen gains achieved with the designed and the commercial stents as well as ratios between the lumen areas after and before stenting are plotted against the normalised longitudinal coordinate in Fig. 5a and 5b, respectively. The longitudinal coordinate was normalised by the plaque length for the single plaque, and by the lengths of the plaques and the gap for two plaques. In general, the designed stents significantly improved the lumen gains, nearly two times larger than those for the commercial stent for both cases, which could also be seen in the comparison of cross-sectional views of the lumen before and after stenting at different positions in Fig. 5 and the artery-plaque after stenting in Fig. 6. For the single plaque, the larger arterial expansion caused by the designed stent resulted in a larger longitudinal shortening of plaque compared to that by the commercial stent. In the case with two focal plaques, their lengths remained the same, but the gap length was shortened after stenting, for both the designed and the commercial stents. Additionally, the lumen area in the middle of the gap was somewhat smaller than the healthy lumen area, i.e., its initial area before stenting.

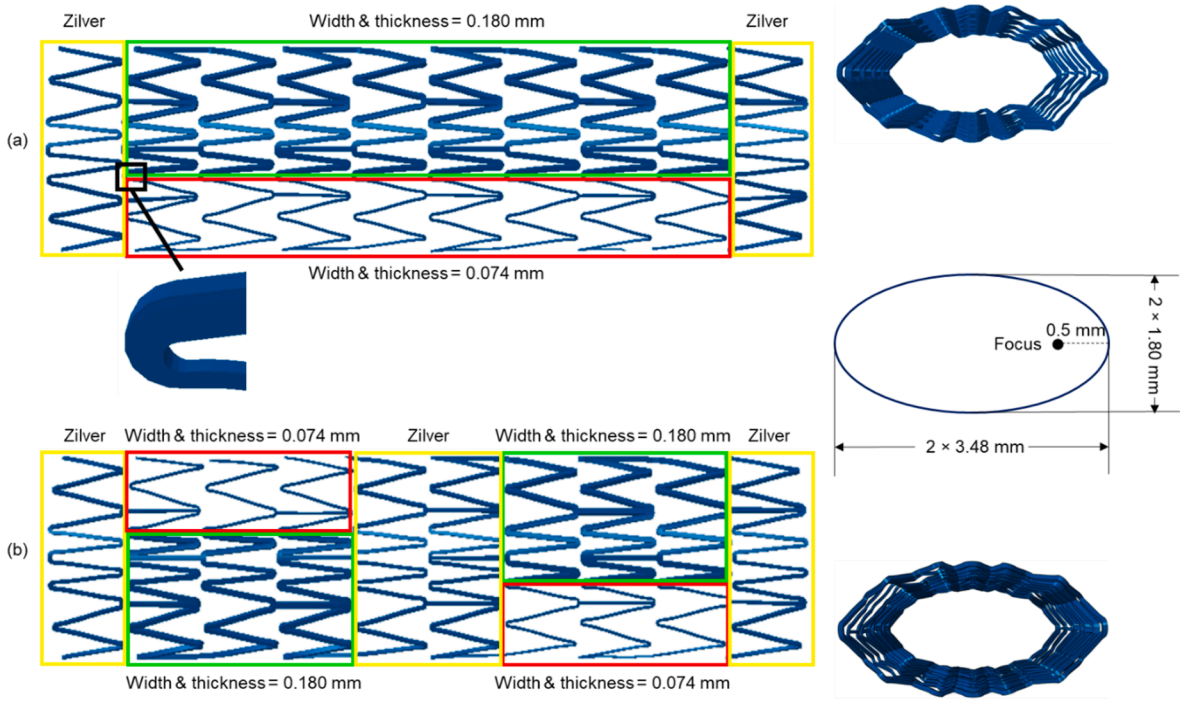

Fig. 4. Top and side views of stent designs for (a) one and (b) two opposite plaques in expanded configuration, with schematics of their oval shape (not to scale).

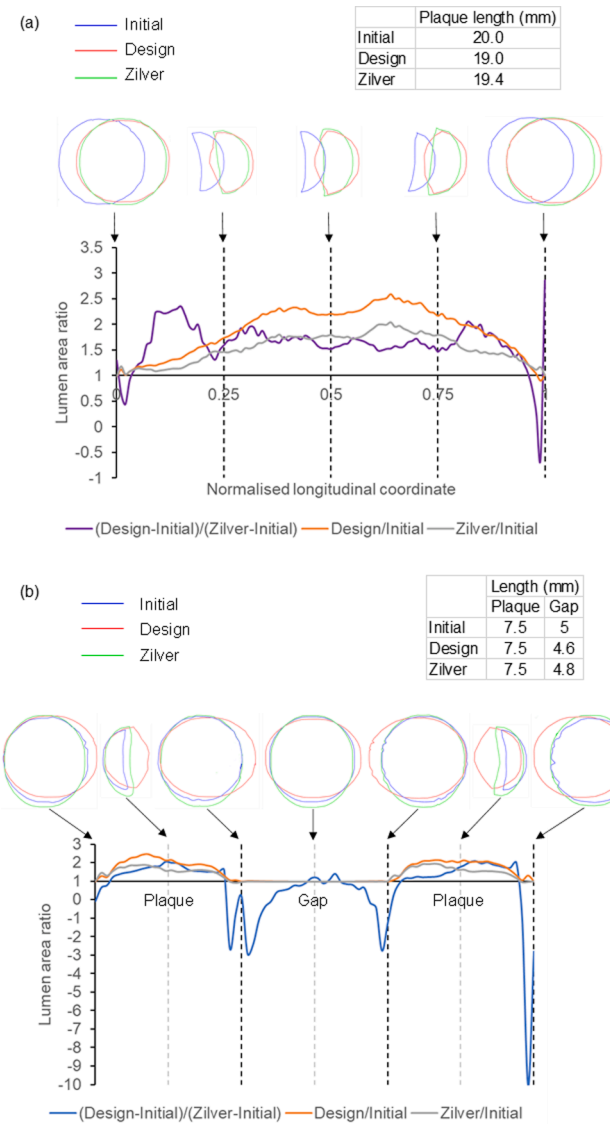

Fig. 5. Ratios of lumen area and their changes in diseased region vs. normalised longitudinal coordinate (lengths of plaques and gap) for (a) one and (b) two opposite focal plaques, with corresponding cross-sectional views of lumen.

4.3. Lumen shape

The cross-sectional views of the lumen in Fig. 5 also demonstrated that the lumen shape was improved by the designed stents in terms of larger expansion in the horizontal direction, compared to the commercial stent, especially for the case of two focal plaques. However, the lumen in the non-diseased region was also expanded in the horizontal and the vertical directions by the designed and the commercial stents, respectively. Additionally, the lumen was straightened more by the designed stents than the commercial stent (Fig. 6).

4.4. Stress in media layer

The maximum von Mises stress in the media layer after deployment of the designed stent (0.024 MPa) was about 2.7 times that for the commercial stent for the single plaque (0.009 MPa; Fig. 7a), whilst about 1.8 times that for the commercial stent for the two plaques (0.032 MPa vs. 0.018 MPa; Fig. 7b). However, the locations of the high-stress regions were different in both cases, i.e., between the focal and the thin-layer plaques for the designed stent, while they were in the focal and the thin-layer plaques for the commercial stent.

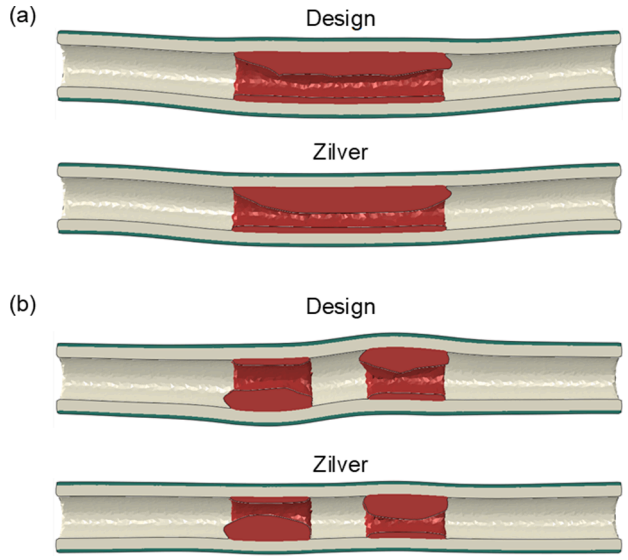

Fig. 6. Arteries with (a) one and (b) two focal plaques (adventitia: green; media: beige; plaque: red) after deployment of designed and commercial stents.

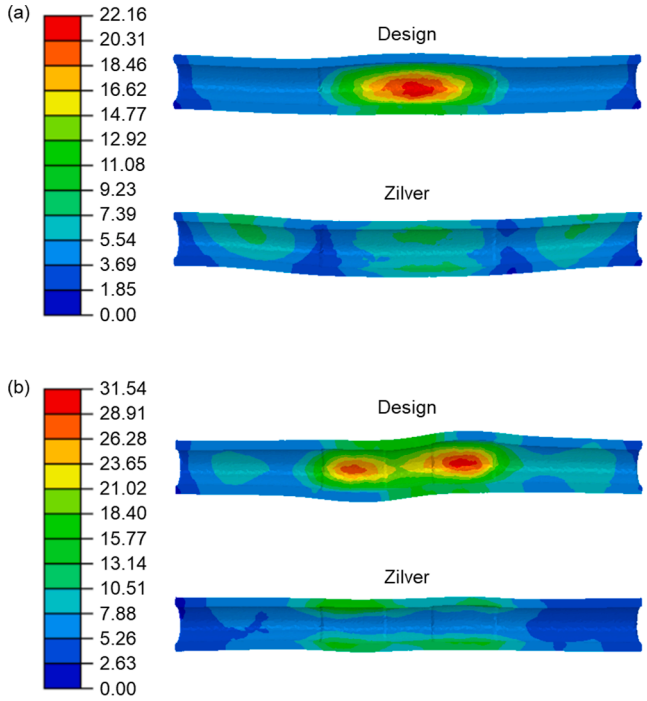

Fig. 7. Contour plots of von Mises stress (in kPa) in media layer after deployment of designed and commercial stents for (a) one and (b) two focal plaques.

5. Discussion

This study developed personalised nitinol stent designs for lesion-specific arteries with one and two opposite focal plaques. The lumen gain and shape were significantly improved by both designed stents compared to the commercial stent. Although higher levels of stress in the media layer were induced by them than by the commercial stent, they achieved the twice larger lumen gain than the commercial stent. Considering a highly non-linear mechanical behaviour of the arterial layers, a stent with a uniform design, like the commercial stent, would generate significantly higher level of stress in the artery if trying to achieve the same lumen gain as the designed stent (see Section 3 in

Supplementary Material). Hence, it could be concluded that the stress level in the media layer was effectively reduced by the designed stents. Another conclusion could be made that the short plaque was easier to expand than the long one, by comparing the lumen gains and the stresses in the media layer induced by the designed stents. The lumen area in the middle of the gap that was smaller than the healthy one for the two focal plaques demonstrated the necessity of placing stent crowns between plaques, even when there was no stenosis. Furthermore, the performance of a thicker Zilver stent was compared with that of the designed stent, proving the latter's advantages (see Section 2 in Supplementary Material).

The lumen gain, the lumen shape, and the stress in the media layer after stenting were used to evaluate the performance of the designed stents in this study. Since restoring the normal blood flow is the top priority in the treatment of the atherosclerosis, the lumen gain is the most significant factor in evaluating the stents' performance. The implantation of the self-expandable stents could leave an up to 24.8% postprocedural diameter stenosis rate in the femoropopliteal arteries, even with pre- and post-dilations (Laird et al., 2014; Liistro et al., 2019, 2013; Werner et al., 2013). Hence, the nitinol stents still need to improve their lumen gain. In addition, the clinical practices desire to restore the lumen shape to a healthy state, and, thus, the lumen shape was considered in the evaluation of the stent's performance as well. Furthermore, a larger lumen gain usually led to higher levels of stress in the media layer, causing larger damage and a higher rate of in-stent restenosis (a reoccurrence of stenosis after stenting), one of the major drawbacks of the stenting treatment. The occurrence of in-stent restenosis after stenting could compromise the large lumen gain in months (He et al., 2020b). Hence, the stress in the media layer after stenting was chosen to evaluate the stents' performance.

Nevertheless, further improvements can be considered in the future work. For both cases, further improvements, such as shorter crown length, can be used in the designs to achieve even larger lumen gains. Although this study was based on a straight artery model, the design ideas were proved highly effective and can be applied to actual patient-specific arteries, which have curvatures, variable diameters and branches. This will be explored in future work. Additionally, shape optimisation should be explored in the future to achieve a more circular lumen shape and a reduced stress level after stenting. The softening effect (damage), a typical behaviour of the plaque and the arterial layers, was not considered in this study. More accurate simulation results and better personalised designs can be produced by including the damage, combined with a tissue-growth model to predict the in-stent restenosis. Also, the stent is basically used to change the lumen towards its healthy shape to achieve a normal or nearly normal blood flow, and, therefore, the flow conditions after stent implantation should be another key point to evaluate the stent design and will need to be investigated in future work. Furthermore, fractures in the implanted stents due to repetitive external force were frequently observed, especially in the femoropopliteal arteries. Hence, future designs should be aimed at improving the fatigue resistance of the stents.

CRediT authorship contribution statement

Ran He: Methodology, Software, Validation, Formal analysis, Investigation, Data Curation, Writing - Original Draft, Visualization. **Liguo Zhao**: Conceptualization, Methodology, Resources, Writing - Review & Editing, Supervision, Project administration, Funding acquisition. **Vadim V. Silberschmidt**: Conceptualization, Writing - Review & Editing, Supervision. **Jiling Feng**: Conceptualization, Resources, Writing - Review & Editing. **Ferdinand Serracino-Inglott**: Conceptualization, Resources, Writing - Review & Editing.

Declaration of Competing Interest

The authors declare that they have no known competing financial interests or personal relationships that could have appeared to influence the work reported in this paper.

Acknowledgement

We acknowledge the support from the EPSRC UK (Grant number: EP/R001650/1; Title: Smart peripheral stents for the lower extremity - design, manufacturing and evaluation). Research data for this paper are available upon request to the project's principal investigator Professor Liguo Zhao at Loughborough University, UK (email: L.Zhao@lboro.ac.uk).

Appendix A. Supplementary data

Supplementary data to this article can be found online at https://doi.org/10.1016/j.jbiomech.2021.110873.

References

Ako, J., Bonneau, H.N., Honda, Y., Fitzgerald, P.J., 2007. Design criteria for the ideal drug-eluting stent. Am. J. Cardiol. 100 (8), S3–S9. https://doi.org/10.1016/j.amjcard.2007.08.016.

Alaimo, G., Auricchio, F., Conti, M., Zingales, M., 2017. Multi-objective optimization of nitinol stent design. Med. Eng. Phys. 47, 13–24. https://doi.org/10.1016/j.medengphy.2017.06.026.

Amirjani, A., Yousefi, M., Cheshmaroo, M., 2014. Parametrical optimization of stent design; a numerical-based approach. Comput. Mater. Sci. 90, 210–220. https://doi.org/10.1016/j.commatsci.2014.04.002.

Auricchio, F., Taylor, R.L., 1997. Shape-memory alloys: Modelling and numerical simulations of the finite-strain superelastic behavior. Comput. Methods Appl. Mech. Eng. 143 (1-2), 175–194. https://doi.org/10.1016/S0045-7825(96)01147-4.

Auricchio, F., Taylor, R.L., Lubliner, J., 1997. Shape-memory alloys: Macromodelling and numerical simulations of the superelastic behavior. Comput. Methods Appl. Mech. Eng. 146 (3-4), 281–312. https://doi.org/10.1016/S0045-7825(96)01232-7.

Azaouzi, M., Lebaal, N., Makradi, A., Belouettar, S., 2013. Optimization based simulation of self-expanding Nitinol stent. Mater. Des. 50, 917–928. https://doi.org/10.1016/j.matdes.2013.03.012.

Blair, R.W., Dunne, N.J., Lennon, A.B., Menary, G.H., 2019. Multi-objective optimisation of material properties and strut geometry for poly(L-lactic acid) coronary stents using response surface methodology. PLoS One 14, e0218768. https://doi.org/10.1371/journal.pone.0218768.

Dassault Systèmes, 2017. 3DEXPERIENCE User Assistance R2017x.

Dordoni, E., Meoli, A., Wu, W., Dubini, G., Migliavacca, F., Pennati, G., Petrini, L., 2014. Fatigue behaviour of nitinol peripheral stents: The role of plaque shape studied with computational structural analyses. Med. Eng. Phys. 36 (7), 842–849. https://doi.org/10.1016/j.medengphy.2014.03.006.

Fereidoonnezhad, B., Naghdabadi, R., Holzapfel, G.A., 2016. Stress softening and permanent deformation in human aortas: Continuum and computational modeling with application to arterial clamping. J. Mech. Behav. Biomed. Mater. 61, 600–616. https://doi.org/10.1016/j.jmbbm.2016.03.026.

Fusaro, M., Cassese, S., Ndrepepa, G., King, L.A., Tada, T., Ott, I., Kastrati, A., 2013. Paclitaxel-coated balloon or primary bare nitinol stent for revascularization of femoropopliteal artery: A meta-analysis of randomized trials versus uncoated balloon and an adjusted indirect comparison. Int. J. Cardiol. 168 (4), 4002–4009. https://doi.org/10.1016/j.ijcard.2013.06.081.

Gasser, T.C., Ogden, R.W., Holzapfel, G.A., 2006. Hyperelastic modelling of arterial layers with distributed collagen fibre orientations. J. R. Soc. Interface 3 (6), 15–35. https://doi.org/10.1098/rsif.2005.0073.

He, H.-P., Weng, J.-C., Zhao, Y., Cai, S.-H., Zhang, X.-L., Yin, H.-H., 2019. Impact of Plaque Calcification and Stent Oversizing on Clinical Outcomes of Atherosclerotic Femoropopliteal Arterial Occlusive Disease Following Stent Angioplasty. Eur. J. Vasc. Endovasc. Surg. 58 (2), 215–222. https://doi.org/10.1016/j.ejvs.2019.01.025.

He, R., Zhao, L., Silberschmidt, V.V., Liu, Y., 2020a. Mechanistic evaluation of long-term in-stent restenosis based on models of tissue damage and growth. Biomech. Model. Mechanobiol. 19 (5), 1425–1446. https://doi.org/10.1007/s10237-019-01279-2.

He, R., Zhao, L.G., Silberschmidt, V.V., Liu, Y., Vogt, F., 2020b. Patient-specific modelling of stent overlap: Lumen gain, tissue damage and in-stent restenosis. J. Mech. Behav. Biomed. Mater. 109, 103836. https://doi.org/10.1016/j.jmbbm.2020.103836.

Holzapfel, G.A., Gasser, T.C., Ogden, R.W., 2000. A new constitutive framework for arterial wall mechanics and a comparative study of material models. J. Elast. 61, 1–48. https://doi.org/10.1023/A:1010835316564.

Khan, M.F., Brackett, D., Ashcroft, I., Tuck, C., Wildman, R., 2017. A novel approach to design lesion-specific stents for minimum recoil. J. Med. Devices, Trans. ASME 11, 011001. https://doi.org/10.1115/1.4034880.

Laird, J.R., Jain, A., Zeller, T., Feldman, R., Scheinert, D., Popma, J.J., Armstrong, E.J., Jaff, M.R., 2014. Nitinol stent implantation in the superficial femoral artery and proximal popliteal artery: Twelve-month results from the complete SE multicenter trial. J. Endovasc. Ther. 21 (2), 202–212. https://doi.org/10.1583/13-4548R.1.

Laird, J.R., Katzen, B.T., Scheinert, D., Lammer, J., Carpenter, J., Buchbinder, M., Dave, R., Ansel, G., Lansky, A., Cristea, E., Collins, T.J., Goldstein, J., Jaff, M.R., 2010. Nitinol stent implantation versus balloon angioplasty for lesions in the superficial femoral artery and proximal popliteal artery: Twelve-month results from the RESILIENT randomized trial. Circ. Cardiovasc. Interv. 3 (3), 267–276. https://doi.org/10.1161/CIRCINTERVENTIONS.109.903468.

Liistro, F., Angioli, P., Porto, I., Ducci, K., Falsini, G., Ventoruzzo, G., Ricci, L., Scatena, A., Grotti, S., Bolognese, L., 2019. Drug-eluting balloon versus drug-eluting stent for complex femoropopliteal arterial lesions: The DRASTICO study. J. Am. Coll. Cardiol. 74, 205–215. https://doi.org/10.1016/j.jacc.2019.04.057.

Liistro, F., Grotti, S., Porto, I., Angioli, P., Ricci, L., Ducci, K., Falsini, G., Ventoruzzo, G., Turini, F., Bellandi, G., Bolognese, L., 2013. Drug-eluting balloon in peripheral intervention for the superficial femoral artery: The DEBATE-SFA randomized trial (Drug Eluting Balloon in Peripheral Intervention for the Superficial Femoral Artery). JACC Cardiovasc. Interv. 6 (12), 1295–1302. https://doi.org/10.1016/j.jcin.2013.07.010.

Maher, E., Creane, A., Sultan, S., Hynes, N., Lally, C., Kelly, D.J., 2011. Inelasticity of human carotid atherosclerotic plaque. Ann. Biomed. Eng. 39 (9), 2445–2455. https://doi.org/10.1007/s10439-011-0331-4.

Ogden, R.W., 1972. Large deformation isotropic elasticity—on the correlation of theory and experiment for incompressible rubberlike solids. Rubber Chem. Technol. 46, 565–584. https://doi.org/10.5254/1.3542910.

Pant, S., Bressloff, N.W., Limbert, G., 2012. Geometry parameterization and multidisciplinary constrained optimization of coronary stents. Biomech Model Mechanobiol 11 (1-2), 61–82. https://doi.org/10.1007/s10237-011-0293-3.

Pant, S., Limbert, G., Curzen, N.P., Bressloff, N.W., 2011. Multiobjective design optimisation of coronary stents. Biomaterials 32 (31), 7755–7773. https://doi.org/10.1016/j.biomaterials.2011.07.059.

Qiu, T., He, R., Abunassar, C., Hossainy, S., Zhao, L.G., 2018. Effect of two-year degradation on mechanical interaction between a bioresorbable scaffold and blood vessel. J. Mech. Behav. Biomed. Mater. 78, 254–265. https://doi.org/10.1016/j.jmbbm.2017.11.031.

Rahdert, D.A., Sweet, W.L., Tio, F.O., Janicki, C., Duggan, D.M., 1999. Measurement of density and calcium in human atherosclerotic plaque and implications for arterial brachytherapy. Cardiovasc. Radiat. Med. 1 (4), 358–367.

Ribeiro, N.S., Folgado, J., Rodrigues, H.C., 2021. Surrogate-based multi-objective design optimization of a coronary stent: Altering geometry toward improved biomechanical performance. Int. j. numer. method. biomed. eng. 37 (6) https://doi.org/10.1002/cnm.v37.610.1002/cnm.3453.

Schiavone, A., Zhao, L.G., 2016. A computational study of stent performance by considering vessel anisotropy and residual stresses. Mater. Sci. Eng. C 62, 307–316. https://doi.org/10.1016/J.MSEC.2016.01.064.

Schillinger, M., Sabeti, S., Loewe, C., Dick, P., Amighi, J., Mlekusch, W., Schlager, O., Cejna, M., Lammer, J., Minar, E., 2006. Balloon angioplasty versus implantation of nitinol stents in the superficial femoral artery. N. Engl. J. Med. 354 (18), 1879–1888. https://doi.org/10.1056/NEJMoa051303.

Schriefl, A.J., Wolinski, H., Regitnig, P., Kohlwein, S.D., Holzapfel, G.A., 2013. An automated approach for three-dimensional quantification of fibrillar structures in optically cleared soft biological tissues. J. R. Soc. Interface 10 (80), 20120760. https://doi.org/10.1098/rsif.2012.0760.

Schriefl, A.J., Zeindlinger, G., Pierce, D.M., Regitnig, P., Holzapfel, G.A., 2012. Determination of the layer-specific distributed collagen fibre orientations in human thoracic and abdominal aortas and common iliac arteries. J. R. Soc. Interface 9 (71), 1275–1286. https://doi.org/10.1098/rsif.2011.0727.

Torres Lebruno, P., Donas, K.P., Fazzini, S., Köhler, C.E., Schwindt, A., Torsello, G., 2020. Use of the Orbital Atherectomy System in Isolated, Chronic Atherosclerotic Lesions of the Popliteal Artery. Vasc. Endovasc. Rev. 3, e11. https://doi.org/10.15420/VER.2020.08.

von Birgelen, C., Klinkhart, W., Mintz, G.S., Papatheodorou, A., Herrmann, J., Baumgart, D., Haude, M., Wieneke, H., Ge, J., Erbel, R., 2001. Plaque distribution and vascular remodeling of ruptured and nonruptured coronary plaques in the same vessel: an intravascular ultrasound study in vivo. J. Am. Coll. Cardiol. 37 (7), 1864–1870. https://doi.org/10.1016/S0735-1097(01)01234-7.

Wang, D., Serracino-Inglott, F., Feng, J., 2021. Numerical simulations of patient-specific models with multiple plaques in human peripheral artery: a fluid-structure interaction analysis. Biomech. Model. Mechanobiol. 20 (1), 255–265. https://doi.org/10.1007/s10237-020-01381-w.

Weisbecker, H., Pierce, D.M., Regitnig, P., Holzapfel, G.A., 2012. Layer-specific damage experiments and modeling of human thoracic and abdominal aortas with non-atherosclerotic intimal thickening. J. Mech. Behav. Biomed. Mater. 12, 93–106. https://doi.org/10.1016/j.jmbbm.2012.03.012.

Werner, M., Piorkowski, M., Thieme, M., Nanning, T., Beschorner, U., Rastan, A., Zeller, T., Scheinert, D., 2013. SUMMIT registry: One-year outcomes after implantation of the epic self-expanding nitinol stent in the femoropopliteal segment. J. Endovasc. Ther. 20 (6), 759–766. https://doi.org/10.1583/13-4430R.1.

Wong, M., Edelstein, J., Wollman, J., Bond, M.G., 1993. Ultrasonic-pathological comparison of the human arterial wall: Verification of intima-media thickness. Arterioscler. Thromb. Vasc. Biol. 13 (4), 482–486. https://doi.org/10.1161/01.ATV.13.4.482.